



City Research Online

City, University of London Institutional Repository

Citation: Klöpfer, D., De Martino, A., Matrasulov, D. & Egger, R. (2014). Scattering theory and ground-state energy of Dirac fermions in graphene with two Coulomb impurities. *European Physical Journal B: Condensed Matter and Complex Systems*, 87(8), 187. doi: 10.1140/epjb/e2014-50414-8

This is the accepted version of the paper.

This version of the publication may differ from the final published version.

Permanent repository link: <https://openaccess.city.ac.uk/id/eprint/4426/>

Link to published version: <https://doi.org/10.1140/epjb/e2014-50414-8>

Copyright: City Research Online aims to make research outputs of City, University of London available to a wider audience. Copyright and Moral Rights remain with the author(s) and/or copyright holders. URLs from City Research Online may be freely distributed and linked to.

Reuse: Copies of full items can be used for personal research or study, educational, or not-for-profit purposes without prior permission or charge. Provided that the authors, title and full bibliographic details are credited, a hyperlink and/or URL is given for the original metadata page and the content is not changed in any way.

City Research Online:

<http://openaccess.city.ac.uk/>

publications@city.ac.uk

Scattering theory and ground-state energy of Dirac fermions in graphene with two Coulomb impurities

Denis Klöpfer¹, Alessandro De Martino², Davron Matrasulov³, and Reinhold Egger¹

¹ Institut für Theoretische Physik, Heinrich-Heine-Universität, D-40225 Düsseldorf, Germany

² Department of Mathematics, City University London, London EC1V 0HB, United Kingdom

³ Turin Polytechnic University in Tashkent, 17 Niyazov Street, 100095 Tashkent, Uzbekistan

the date of receipt and acceptance should be inserted later

Abstract. We study the physics of Dirac fermions in a gapped graphene monolayer containing two Coulomb impurities. For the case of equal impurity charges, we discuss the ground-state energy using the linear combination of atomic orbitals (LCAO) approach. For opposite charges of the Coulomb centers, an electric dipole potential results at large distances. We provide a nonperturbative analysis of the corresponding low-energy scattering problem.

PACS. 72.80.Vp Electronic transport in graphene – 73.22.Pr Electronic structure of graphene

1 Introduction

The amazing properties of graphene monolayers have attracted much attention in physics and material science over the past decade. It is by now well established that in the vicinity of the charge neutrality point, electronic quasi-particle excitations correspond to two-dimensional (2D) Dirac fermions [1]. In the presence of a bulk gap, Δ , these are massive fermions. The gap can be caused by various different mechanisms. To list just a few, let us mention strain-engineered gaps [2], artificially designed spin-orbit interaction processes [3], and strong Coulomb effects causing an excitonic insulator phase [4]. Additional ways to open a gap come from superlattices that arise when the graphene layer is deposited on a substrate [5,6], or simply due to the transverse finite-size gap in graphene nanoribbons [1]. Graphene monolayers thus imply new possibilities for experimentally accessing relativistic quantum phenomena within a readily available table-top setting.

A prime example for such a relativistic quantum effect concerns *supercriticality*: In the presence of a Coulomb impurity of charge $Q = Ze$ (where the electron has charge $-e$), the attractive $1/r$ potential induces bound states with energy E inside the gap, $|E| < \Delta$. For sufficiently large $Z > Z_c$, these bound states are predicted to “dive” into the filled Dirac sea [4, 7, 8, 9, 10, 11, 12, 13], whereby the nucleus captures an electron to reduce its charge. In conventional realizations, the large value of the critical charge, $Z_c \approx 170$, renders the experimental observation of supercriticality prohibitively difficult [14, 15]. In graphene, the Fermi velocity $v_F \ll c$ takes the role of the speed of light c , and therefore the effective fine structure constant becomes of order $\alpha = e^2/\hbar v_F \approx 1$ instead of $e^2/\hbar c \simeq 1/137$. As a

result, in graphene one expects a much smaller value for the critical charge, $Z_c \approx 1$. Indeed, this reduction in Z_c has already allowed one to observe supercriticality by tunneling spectroscopy measurements in graphene monolayers [16, 17]. In those experiments, a Coulomb center was artificially created by pushing together charged Co adatoms [13, 16] with the help of a scanning tunneling microscope (STM) tip. A similar procedure has also been successfully used for Ca adatoms [17]. Importantly, by local gating it is possible to vary the charge Q of the resulting cluster (including the sign) in a controlled manner.

These recent developments allow one to envision new types of artificial molecules, composed of N_Z nuclei with designed charges and N electrons bound to them. Since the electron dynamics is now governed by the Dirac equation, such molecules may realize a relativistic 2D counterpart to conventional molecules, with potentially much stronger correlation effects. Note that for different signs of the nuclear charges, one has a polar molecule. We here study the simplest problem of this class, which is defined by just one 2D Dirac fermion, $N = 1$, in the field of two static Coulomb centers, $N_Z = 2$, separated by a distance R . The Coulomb centers have charges Q_1 and Q_2 , where we restrict ourselves to symmetric and antisymmetric configurations, $Q_2 = \pm Q_1$. The symmetric case represents a relativistic 2D cousin of the well-known H_2^+ problem [18], while the antisymmetric case corresponds to a polar molecule, i.e., an electric dipole. The main theoretical difficulty in treating this problem is that the 2D Dirac equation with a two-center potential does not separate in any known orthogonal coordinate system.

First, for equal charges, $Q_{1,2} = Q = Ze$, we have a symmetric two-center problem for Dirac fermions in

graphene. As recently discussed in Ref. [19], one then encounters a supercritical instability again. Indeed, for $R \rightarrow 0$, the problem reduces to a single Coulomb impurity with charge $2Q$, while for $R \rightarrow \infty$, we recover the charge- Q single-impurity problem. Assuming a subcritical value of Q such that $1/2 < \zeta < 1$, with $\zeta = Z/Z_c$, one expects that by pushing together the Coulomb centers, supercriticality emerges below some critical distance, $R < R_{\text{cr}}$. The idea to induce supercriticality by bringing together two Coulomb centers has already been discussed in the 1970s for colliding heavy nuclei [20,21,22], and is implicitly behind the recent graphene experiments [16,17]. The critical distance for the graphene case was computed in Ref. [19] by an asymptotic matching procedure, leading to the transcendental equation

$$2\sqrt{1-\zeta^2} - 1 = \frac{zK'_{i\gamma}(z)}{K_{i\gamma}(z)}, \quad z = 2\sqrt{\zeta R_{\text{cr}}/R_{\Delta}}, \quad (1)$$

with $\gamma = \sqrt{4\zeta^2 - 1}$, $R_{\Delta} = \hbar v_F/\Delta$, and the Macdonald function $K_{i\gamma}(z)$ with imaginary order [23,24]. We here develop an alternative description of this phenomenon based on the “linear combination of atomic orbitals” (LCAO) approach, which is commonly used in molecular physics [18]. The corresponding two-center Dirac problem in three dimensions (3D) has been studied by the LCAO technique in Refs. [25,26].

For opposite charges, $Q_2 = -Q_1 = Q$, the two-center potential reduces for large distances, $r \gg R$, to the potential of an *electric dipole* with dipole moment $P = QR$,

$$V_d(r, \theta) = -\frac{eP \cos \theta}{r^2}, \quad (2)$$

where θ is the azimuthal angle between \mathbf{r} and the dipole axis. V_d is referred to below as the “point-like dipole” potential. A similar $1/r^2$ potential also describes the conical singularities near graphene wrinkles [27]. Recently, we have presented a related study of the dipolar two-center problem in graphene [28], where we have analyzed the bound states induced by the dipole, see also Sec. 4.1 below. It turns out that an arbitrarily weak dipole can already bind infinitely many states. This is in contrast to 3D Schrödinger fermions, where the dipole is able to capture bound states only when P exceeds a finite critical strength [29,30,31,32,33]. However, for the 2D Schrödinger case, the critical dipole strength vanishes as well [32]. In Ref. [28], we have – albeit very briefly – also discussed the scattering problem in graphene, using the dipolar two-center Dirac equation within the perturbative Born approximation. The resulting scattering state implies a completely isotropic transport cross-section. Within the Born approximation, this predicts that charge transport is independent of the angle between current flow and dipole direction. In the present work, we elaborate on the scattering problem also beyond the Born approximation, including the non-perturbative low-energy regime.

The structure of the remainder of this article is as follows. In Sec. 2, we introduce the model and discuss its symmetries. Sec. 3 provides a discussion of our Dirac-LCAO calculations for the symmetric two-center problem.

In Sec. 4, we then describe the scattering theory results for the dipolar potential with opposite nuclear charges. We finally offer some concluding remarks in Sec. 5.

2 Model

Throughout this paper, we study 2D Dirac fermions with a mass gap Δ in the presence of a static two-center potential. Using units with $\hbar = e = 1$, the Hamiltonian reads [1]

$$H = -iv_F \partial_x \sigma_x - iv_F \partial_y \sigma_y + \Delta \sigma_z + V. \quad (3)$$

The Pauli matrices $\sigma_{x,y,z}$ act in sublattice space, corresponding to the two atoms in the elementary cell of graphene’s honeycomb lattice. Following standard arguments, we consider a single K point (“valley”) and a single electron spin projection only [1]. It is worth mentioning that Eq. (3) also describes other Dirac materials, e.g., the “molecular graphene” resulting from the deposition of CO molecules on a copper surface as described in Ref. [34], or the recently discovered surface states of topological insulator materials such as Bi_2Se_3 or Bi_2Te_3 [35]. The Hamiltonian (3) acts on states with two spinor components, $\Psi(\mathbf{r}) = (\eta, \chi)^T$. With the nuclear charges $Z_{1,2}$, the two-center potential V in Eq. (3) reads

$$V(x, y) = -\frac{Z_1}{r_1} - \frac{Z_2}{r_2}, \quad (4)$$

with the distances $r_{1,2}$ of the electron to the two Coulomb centers. Assuming that the centers are at $y = 0$ and $x = \mp R/2$, resp., we have

$$r_{1,2} = \sqrt{(x \pm R/2)^2 + y^2}. \quad (5)$$

The dipole case is realized for $Z_2 = -Z_1 = Z$, with dipole moment $P = ZR$. For $Z_1 = Z_2 = Z$, we instead have a symmetric two-center problem.

Let us next discuss the symmetry properties of this system. For $Z_1 = Z_2$, the Hamiltonian is invariant under a π -rotation exchanging the two Coulomb centers. Indeed, with the total angular momentum operator,

$$J_z = -i\partial_\theta + \frac{\sigma_z}{2}, \quad (6)$$

the unitary operator $\mathcal{R}_\pi = e^{i\pi J_z}$ generates the shift $\theta \rightarrow \theta + \pi$ and commutes with the Hamiltonian, $[H, \mathcal{R}_\pi]_- = 0$. The spinor is thereby mapped to

$$\Psi(x, y) \rightarrow \mathcal{R}_\pi \Psi = i\sigma_z \Psi(-x, -y). \quad (7)$$

We note that the single-valley Hamiltonian (3) is *not* invariant under the reflection $x \rightarrow -x$, which maps left- to right-handed quasi-particles.

In the dipolar case, $Z_2 = -Z_1$, the Hamiltonian does not have the above symmetry, but instead it maps to $-H$ by the unitary transformation $U = \sigma_x \mathcal{R}_x$, where \mathcal{R}_x performs the reflection $x \rightarrow -x$. Indeed, we find $U H U^\dagger = -H$, which implies a particle-hole-like symmetry of the

entire spectrum. By virtue of this unitary transformation, out of an eigenstate $\Psi_E(x, y)$ at energy E , one immediately obtains a partner state at energy $-E$,

$$\Psi_{-E}(x, y) = U\Psi_E(x, y) = \sigma_x\Psi_E(-x, y). \quad (8)$$

All solutions to the dipolar two-center Dirac equation therefore come in $\pm E$ pairs, and it is sufficient to study only, say, $E < 0$. We note that there are no $E = 0$ solutions [28].

3 LCAO approach for symmetric two-center problem

In this section, we present ground-state results obtained from the LCAO approach for the symmetric two-center Dirac problem in 2D. The corresponding potential V is given in Eq. (4) with $Z_1 = Z_2 = Z$. The LCAO approximation solves the Dirac equation in a truncated subspace, where only the lowest single-impurity bound state near each center is retained. This approximation is expected to yield accurate ground-state energies for large R [25,26], where the molecular ground state is well approximated in terms of atomic orbitals. In addition, as we show below, the exact result for $R \rightarrow 0$ is also captured by the LCAO solution.

3.1 Single-impurity ground state

Since the LCAO method employs a superposition of states localized near one of the centers, we first summarize the known single-impurity solution for the lowest bound state [7,8,11]. Taking a single impurity of charge Z , i.e., using $V = -Z/r$ in Eq. (3), the lowest bound state has the energy $\xi\Delta$, with

$$\xi = \sqrt{1 - 4Z^2}. \quad (9)$$

In the absence of short-distance regularization, the supercritical threshold is reached at $Z_c = 1/2$ [11], and we assume $Z < Z_c$ henceforth. The corresponding spinor is an eigenstate of the total angular momentum operator J_z in Eq. (6), with eigenvalue $1/2$. Using the lengthscale $R_\Delta = \hbar v_F/\Delta$, and ξ in Eq. (9), it reads

$$\begin{aligned} \Psi_0(r, \theta) = & \frac{2Z}{\sqrt{\pi}\Gamma(1+\xi)R_\Delta} \left(\frac{4Zr}{R_\Delta} \right)^{(\xi-1)/2} \\ & \times e^{-2Zr/R_\Delta} \begin{pmatrix} \sqrt{1+\xi} \\ ie^{i\theta}\sqrt{1-\xi} \end{pmatrix}, \end{aligned} \quad (10)$$

where $\Gamma(z)$ is the Gamma function.

3.2 LCAO scheme

Using the kinetic (Dirac) Hamiltonian $H_0 = H - V$ in Eq. (3), we first re-write the Hamiltonian as

$$H = H_0 - Z_{\text{eff}} \left(\frac{1}{r_1} + \frac{1}{r_2} \right) - \frac{\delta Z_1}{r_1} - \frac{\delta Z_2}{r_2}, \quad (11)$$

where $\delta Z_{1,2} = Z_{1,2} - Z_{\text{eff}}$, and $r_{1,2}$ has been defined in Eq. (5). (We will put $Z_1 = Z_2$ later on.) While Eq. (11) is, of course, exact for arbitrary effective charge Z_{eff} , the LCAO approximation obtains a ground-state energy, E , that still depends on the value of Z_{eff} . The final LCAO ground-state energy is then obtained by minimizing $E(Z_{\text{eff}})$ with respect to the variational parameter Z_{eff} .

Following the standard LCAO approach [18], we expand the ground state $|\Phi\rangle$ of Eq. (11) in terms of atomic orbitals, $|1\rangle$ and $|2\rangle$, centered near the Coulomb impurity at $(\mp R/2, 0)$, respectively, i.e., $|\Phi\rangle = v_1|1\rangle + v_2|2\rangle$. The atomic orbitals are chosen as single-impurity states (10), where the energy $\xi\Delta$ follows from Eq. (9) with $Z \rightarrow Z_{\text{eff}}$. The Dirac equation is thereby reduced to a linear 2×2 equation for (v_1, v_2) , and the energy $E = E(Z_{\text{eff}})$ follows from the condition

$$\det \begin{pmatrix} H_{11} - E & H_{12} - SE \\ H_{21} - SE & H_{22} - E \end{pmatrix} = 0, \quad (12)$$

with the overlap integral

$$S = \langle 1|2\rangle = \langle 2|1\rangle. \quad (13)$$

Note that the single-impurity state (10) is normalized, and therefore we have $\langle 1|1\rangle = \langle 2|2\rangle = 1$. Defining the Coulomb integral,

$$C = \langle 1|r_2^{-1}|1\rangle = \langle 2|r_1^{-1}|2\rangle, \quad (14)$$

and the resonance integral,

$$A = \langle 1|r_{1,2}^{-1}|2\rangle = \langle 2|r_{1,2}^{-1}|1\rangle, \quad (15)$$

and using the relation

$$\langle 1|r_1^{-1}|1\rangle = 4Z_{\text{eff}}\Delta/\xi, \quad (16)$$

all matrix elements in Eq. (12) can be written in compact form,

$$\begin{aligned} H_{11} &= \xi\Delta - 4Z_{\text{eff}}\delta Z_1\Delta/\xi - Z_2C, \\ H_{12} &= \xi S\Delta - (\delta Z_1 + Z_2)A, \\ H_{21} &= \xi S\Delta - (Z_1 + \delta Z_2)A, \\ H_{22} &= \xi\Delta - Z_1C - 4Z_{\text{eff}}\delta Z_2\Delta/\xi. \end{aligned} \quad (17)$$

While in the 3D Dirac problem, the quantities S , C , and A can be directly evaluated [25,26], the 2D case is, unfortunately, more involved.

3.3 Overlap, Coulomb, and resonance integrals

In order to compute the quantities S , C , and A , it is useful to employ elliptic coordinates. Denoting the distances of the electron from the two centers by $r_{1,2}$, see Eq. (5), elliptic coordinates are defined by [23]

$$\mu = \frac{r_1 + r_2}{R} \in [1, \infty), \quad \nu = \frac{r_1 - r_2}{R} \in [-1, 1], \quad (18)$$

where the standard cartesian coordinates are

$$x = \frac{R}{2}\mu\nu, \quad y = \pm \frac{R}{2}\sqrt{(\mu^2 - 1)(1 - \nu^2)}. \quad (19)$$

The \pm sign is chosen according to whether $\mathbf{r} = (x, y)$ is in the upper or lower half-plane: the transformation between cartesian and elliptic coordinates is only one-to-one in each half-plane. The segment $\mu = 1$ with $-1 \leq \nu \leq 1$ then corresponds to the points on the x -axis between $-R/2$ and $+R/2$, while the regions $x \leq -R/2$ ($x \geq R/2$) are covered by $\nu = -1$ ($\nu = 1$) with $1 \leq \mu < \infty$, respectively. We note that the Jacobian determinant,

$$\det J = \mp \frac{R^2}{4} \frac{\mu^2 - \nu^2}{\sqrt{(\mu^2 - 1)(1 - \nu^2)}}, \quad (20)$$

is singular along the full x -axis. In terms of elliptic coordinates, the sought quantities (S , C , and A) are thereby expressed as integrals over μ and ν .

Let us start with the overlap integral S in Eq. (13). Using the abbreviations $\xi = \sqrt{1 - 4Z_{\text{eff}}^2}$,

$$\mathcal{N} = \frac{4u^{1+\xi}}{\pi\Gamma(1+\xi)}, \quad u = \frac{2RZ_{\text{eff}}}{R_{\Delta}}, \quad (21)$$

it takes the form

$$S = \mathcal{N} \int_1^\infty d\mu \int_{-1}^1 d\nu \frac{(\mu^2 - \nu^2)^{(\xi-1)/2} e^{-u\mu}}{\sqrt{(\mu^2 - 1)(1 - \nu^2)}} \times [\mu^2 - 1 + \xi(1 - \nu^2)]. \quad (22)$$

By virtue of the auxiliary relation

$$\int_{-1}^1 d\nu (1 - \nu^2)^{\pm 1/2} \left(1 - \frac{\nu^2}{\mu^2}\right)^s = \frac{2\pi}{3 \pm 1} F\left(\frac{1}{2}, -s; \frac{3 \pm 1}{2}; \frac{1}{\mu^2}\right), \quad (23)$$

the ν -integration can be performed. In the next step, we employ a standard series representation for the hypergeometric function $F(a, b; c; d)$ [23], where the resulting summation commutes with the μ -integration in Eq. (22). After this integration, we encounter the function

$$\mathcal{I}(s, u) = \int_1^\infty d\mu \frac{\mu^s e^{-u\mu}}{\sqrt{\mu^2 - 1}}, \quad (24)$$

which can be evaluated in closed form. With the Pochhammer symbol $(a)_n$, recursively defined by $(a)_n/(a)_{n-1} = a + n - 1$ and $(a)_0 = 1$ [23], we arrive at a rapidly convergent series,

$$S = \pi\mathcal{N} \sum_{n=0}^\infty \frac{(1/2)_n}{n!} \left\{ \frac{\left(-\frac{1+\xi}{2}\right)_n}{(1)_n} \mathcal{I}(\xi + 1 - 2n, u) - \frac{1 - \xi}{2} \frac{\left(\frac{1-\xi}{2}\right)_n}{(2)_n} \mathcal{I}(\xi - 1 - 2n, u) \right\}. \quad (25)$$

By very similar steps, we also obtain the Coulomb integral,

$$C = \frac{2\pi\mathcal{N}}{R} \sum_{n=0}^\infty \frac{(1/2)_n}{n!} \left\{ \frac{\left(-\frac{\xi+1}{2}\right)_n}{(1)_n} \mathcal{I}(\xi - 2n, u) - \frac{1 - \xi}{2} \frac{\left(\frac{3-\xi}{2}\right)_n}{(2)_n} \mathcal{I}(\xi - 2 - 2n, u) \right\}. \quad (26)$$

Concerning the resonance integral A , one has to proceed in a different manner. Elliptic coordinates yield the expression

$$A = \frac{4\mathcal{N}}{R} \int_1^\infty d\mu \int_{-1}^1 d\nu \frac{(\mu + \nu)^\xi e^{-u(\mu+\nu)}}{\sqrt{(\mu^2 - 1)(1 - \nu^2)}}. \quad (27)$$

Expanding $(1 + \nu/\mu)^\xi = \sum_{n=0}^\infty \binom{\xi}{n} (\nu/\mu)^n$, the ν -integrals are done using

$$\int_{-1}^1 d\nu \frac{e^{-u\nu} \nu^n}{\sqrt{1 - \nu^2}} = (-1)^n \pi \frac{\partial^n I_0(u)}{\partial u^n}, \quad (28)$$

where I_0 is the modified Bessel function [23]. The subsequent μ -integration then leads to expressions as in Eq. (24), and we get the series representation

$$A = \frac{4\pi\mathcal{N}}{R} \sum_{n=0}^\infty (-1)^n \binom{\xi}{n} \mathcal{I}(\xi - n, u) \frac{\partial^n I_0(u)}{\partial u^n}, \quad (29)$$

which is also rapidly convergent. We now put $Z_1 = Z_2 = Z$ and turn to the LCAO results for the ground-state energy.

3.4 LCAO results

Using the above series representations for S , C , and A , it is numerically straightforward to obtain the LCAO estimate for the ground-state energy $E(Z_{\text{eff}})$ for given Z_{eff} . We then determine the minimal energy, realized for $Z_{\text{eff}} = Z^*$, where the numerical search is aided by noting that $E(Z_{\text{eff}})$ depends quadratically on $Z_{\text{eff}} - Z^*$. The optimal value, Z^* , is shown in the inset of Fig. 1. The main panel of Fig. 1 gives the corresponding ground-state energy for $Z = 0.2$, where supercriticality is never reached since we have chosen a value with $2Z < Z_c = 1/2$, i.e., $E(R) > -\Delta$ for all values of the impurity distance R . We also observe that the LCAO ground-state energy, $E(R)$, matches the expected single-impurity values in Eq. (9) in both limits, namely (i) for $R \rightarrow \infty$ with impurity charge Z , where we have two decoupled copies of the single-impurity problem, and (ii) for $R \rightarrow 0$, where both centers conspire to form a single Coulomb impurity of charge $2Z$. Furthermore, the inset illustrates that the optimal effective charge Z^* nicely matches both limits as well.

Choosing larger Z such that $\zeta = Z/Z_c = 2Z$ is within the bounds $1/2 < \zeta < 1$, the supercritical regime can be realized by decreasing R through a transition value, $R = R_{\text{cr}}$. At the critical distance, the ground-state energy reaches the Dirac sea, $E(R_{\text{cr}}) = -\Delta$, and for $R < R_{\text{cr}}$, the two-center system with subcritical individual impurity charge becomes supercritical. The LCAO prediction for the critical distance R_{cr} is shown as a function of ζ in the main panel of Fig. 2, where the inset illustrates our strategy for obtaining R_{cr} .

The LCAO results in Fig. 2 are rather similar to the predictions of Eq. (1) and indicate that, in practice, Z has to be chosen quite close to $Z_c = 1/2$, since otherwise R_{cr}

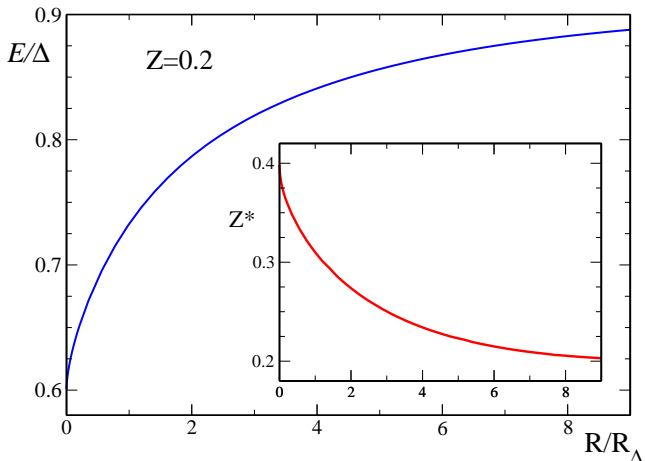


Fig. 1. Main panel: LCAO result for the ground-state energy, E , vs impurity distance R (which is given in units of $R_\Delta = \hbar v_F/\Delta$), for the two-center potential with $Z_1 = Z_2 = Z = 0.2$. Inset: Optimal choice for the variational parameter, $Z_{\text{eff}} = Z^*$, determining the LCAO ground state, as a function of R .

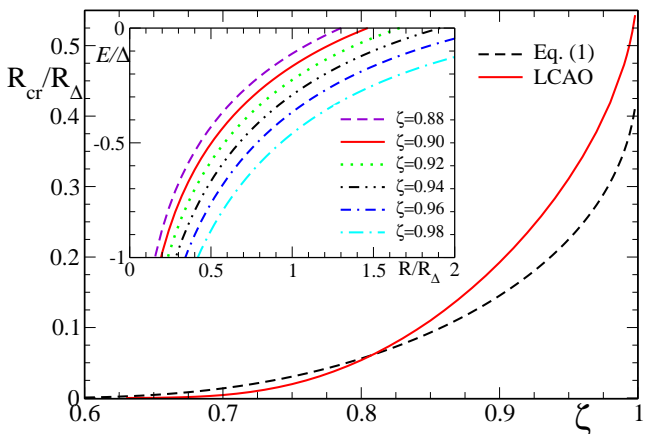


Fig. 2. Main panel: Critical distance R_{cr} vs $\zeta = Z/Z_c$, for the symmetric two-center problem. The red curve gives the LCAO result, and the black curve is the corresponding asymptotic matching result (1). Inset: LCAO ground state energy vs R , for various ζ . Once $E(R)$ reaches $-\Delta$, the level “dives” into the lower continuum and turns supercritical.

becomes extremely small. This conclusion seems also in agreement with the reported experimental observations of supercriticality [16, 17], where different ions first had to be pushed closely together, thereby forming charged clusters, before supercriticality appears.

4 Dipolar two-center potential

In this section, we turn to the dipolar case, $Z_2 = -Z_1 = Z$ in Eq. (4). We first analyze the conditions for bound states in this potential, thereby also summarizing those results of

Ref. [28] that are relevant for the subsequent discussion. We then turn to the scattering problem. After presenting the general scattering state for the Dirac problem in Sec. 4.2, we study the results of the Born approximation in Sec. 4.3. This approximation holds when the energy of the scattering state does not approach the band edge; otherwise a nonperturbative analysis is required and will be given in Sec. 4.4.

4.1 Bound state spectrum

We start by analyzing the possibility of bound states induced by the dipolar two-center potential. For the corresponding Schrödinger case, a scaling argument shows [32] that all energy eigenvalues must be of the form $E_{\text{Schr}} = (mR^2)^{-1}\mathcal{F}(mP)$ [recall that we use units with $\hbar = e = 1$], where m is the mass of the electron, the dipole moment is $P = ZR$, and \mathcal{F} denotes a dimensionless one-parameter scaling function. The critical dipole strength allowing for bound states follows from the condition $\mathcal{F} = 0$, which does not involve Z and R separately but only the combination $P = ZR$. This implies that both the two-center potential and the point-like dipole form (with $P = ZR$) lead to the same critical coupling. For the 2D case, this critical value is zero [32].

Repeating this scaling argument for the Dirac case, we see that the energy eigenvalues can be written as $E_{\text{Dirac}} = \Delta\mathcal{G}(P\Delta/v_F^2, R\Delta/v_F)$, with a *two-parameter* scaling function \mathcal{G} . The condition for bound states now becomes $\mathcal{G} = \pm 1$, which implies that, in general, the critical dipole coupling still depends on the impurity distance R . However, for $R\Delta/v_F \gg 1$, \mathcal{G} effectively becomes a one-parameter scaling function again, and the critical coupling is independent of R . In this subsection, we assume that this limit is realized.

Noting that the entire spectrum is particle-hole symmetric, our analysis in Ref. [28] showed that weakly bound states of energy $E = \pm(\Delta - \epsilon)$, for $0 < \epsilon \ll \Delta$, are arranged in infinite “towers”. In each tower, all bound states have the same “angular momentum”, $j = 0, 1, 2, \dots$; the latter differs from true angular momentum which is not conserved due to the lack of isotropy. Different towers are also labeled by a parity eigenvalue, $\kappa = \pm$, describing the symmetry of the solution under the spatial inversion $x \rightarrow -x$, where the dipole points along the x -axis. Allowed towers have to satisfy $j + \kappa \geq 0$. For given (j, κ) , the respective tower of bound states only exists if P exceeds a critical value, $P > P_{j, \kappa}$. Once this is the case, the dipole hosts infinitely many states belonging to this tower. Remarkably, since $P_{0, +} = 0$, one always has at least one tower. For a mathematically rigorous discussion of these points, we refer to Ref. [36]. The threshold couplings $P_{j, \kappa}$ are ordered as $P_{0, +} < P_{1, -} < P_{1, +} < P_{2, -} < \dots$, and using the approach of Ref. [29], we found that for $j > 0$ a very good approximation is given by [28]

$$P_{j, \kappa} \simeq \frac{\Gamma^4(1/4) v_F^2}{64\pi} \frac{1}{\Delta} \left[\left(2j + \frac{\kappa}{2} \right)^2 - \frac{1}{6\pi} \right]. \quad (30)$$

Bound states within the same tower obey the scaling hierarchy ($n = 1, 2, \dots$)

$$\frac{\epsilon_{n+1}}{\epsilon_n} = \exp\left(-\frac{2\pi}{s_{j,\kappa}}\right), \quad (31)$$

with the numbers ($P > P_{j,\kappa}$)

$$s_{j,\kappa} \simeq \begin{cases} \sqrt{2}P\Delta, & (j, \kappa) = (0, +), \\ 0.956\sqrt{(P - P_{j,\kappa})\Delta}, & j > 0. \end{cases} \quad (32)$$

For $n \rightarrow \infty$, all bound states accumulate near the gap edges according to the universal Efimov scaling law (31). This law also describes bound states of three bosons in free space [37, 38, 39].

4.2 Scattering state

Let us now turn to scattering states. For an incoming plane wave with momentum $\mathbf{k} = k(\cos \phi_{\mathbf{k}}, \sin \phi_{\mathbf{k}})$, using $\sigma = \pm$ to distinguish positive and negative energy solutions, the Dirac scattering state has the energy

$$E_{\mathbf{k},\sigma} = \sigma\sqrt{\Delta^2 + v_F^2 k^2}. \quad (33)$$

The asymptotic form of the state for $r \gg R$ contains an outgoing spherical wave,

$$\Psi_{\mathbf{k},\sigma}(r, \theta) \simeq e^{i\mathbf{k}\cdot\mathbf{r}}U_{\mathbf{k},\sigma} + f(\theta, \phi_{\mathbf{k}}) \frac{e^{ikr}}{\sqrt{-ir}} U_{k\hat{e}_r, \sigma}, \quad (34)$$

with $\mathbf{r} = r\hat{e}_r$, $\hat{e}_r = (\cos \theta, \sin \theta)$, and the spinor [1]

$$U_{\mathbf{k},\sigma} = \frac{1}{\sqrt{2|E_{\mathbf{k},\sigma}|}} \begin{pmatrix} \sqrt{|E_{\mathbf{k},\sigma} + \Delta|} e^{-i\phi_{\mathbf{k}}/2} \\ \sigma\sqrt{|E_{\mathbf{k},\sigma} - \Delta|} e^{i\phi_{\mathbf{k}}/2} \end{pmatrix}. \quad (35)$$

Below, we first discuss the Born approximation for the scattering amplitude $f(\theta, \phi_{\mathbf{k}})$, followed by a nonperturbative treatment. This becomes necessary when the energy approaches the gap, but is analytically possible only for the point-like dipole potential, V_d . For such a $1/r^2$ potential, it is well-known that a short-distance regularization scheme is required to prevent the usual fall-to-the-center problem [40].

4.3 Born approximation

Treating the scattering problem within perturbation theory, the outgoing part of the scattering state reads [8, 41]

$$\begin{aligned} \Psi_{\mathbf{k},\sigma}^{(\text{out})}(\mathbf{r}) = & - \int dx' dy' G_{\mathbf{k},\sigma}(\mathbf{r} - \mathbf{r}') \left(-i\sigma_x \partial_{x'} \right. \\ & \left. - i\sigma_y \partial_{y'} + \Delta\sigma_z + E_{\mathbf{k},\sigma} \right) V(\mathbf{r}') e^{i\mathbf{k}\cdot\mathbf{r}'} U_{\mathbf{k},\sigma}, \end{aligned} \quad (36)$$

with $\mathbf{r}' = (x', y')$ and

$$G_{\mathbf{k},\sigma}(\mathbf{r}) = \frac{i\sigma}{4} H_0^{(1)}(kr) \simeq \frac{i\sigma}{2} \frac{e^{ikr - i\pi/4}}{\sqrt{2\pi kr}}, \quad (37)$$

where the second expression uses the asymptotic form of the Hankel function $H_0^{(1)}$ [23]. Here, and in the remainder of the paper, we often use units with $v_F = 1$. The results in this subsection are obtained by using the full two-center potential $V(\mathbf{r})$ with $Z_2 = -Z_1$, see Eq. (4).

The Born approximation for the scattering amplitude then follows by comparing Eqs. (36) and (34). The result is expressed in terms of the Fourier transform of V , which is given by

$$\tilde{V}(\mathbf{q}) = \frac{4\pi iP}{qR} \sin\left(\frac{q_x R}{2}\right), \quad (38)$$

with $P = ZR$ and the momentum exchange $\mathbf{q} = k\hat{e}_r - \mathbf{k}$. We note that

$$\begin{aligned} q &= |\mathbf{q}| = 2k|\sin[(\theta - \phi_{\mathbf{k}})/2]|, \\ q_x &= -\sigma' q \sin[(\theta + \phi_{\mathbf{k}})/2], \end{aligned} \quad (39)$$

where $\sigma' = \pm$ is the sign of $\sin[(\theta - \phi_{\mathbf{k}})/2]$. The scattering amplitude in Born approximation then reads

$$f(\theta, \phi_{\mathbf{k}}) = -\sqrt{\frac{k}{8\pi v_F^2}} \tilde{V}(\mathbf{q}) b(\theta - \phi_{\mathbf{k}}; E_{\mathbf{k},\sigma}), \quad (40)$$

where

$$b(\varphi; E) = \sum_{\pm} e^{\pm i\varphi/2} \left| \frac{E + \Delta}{E - \Delta} \right|^{\pm 1/2} \quad (41)$$

is specific for Dirac fermions [8]. For $|E| \gg \Delta$, Eq. (41) simplifies to $b = 2 \cos(\varphi/2)$, reflecting the absence of backscattering [1] for Dirac fermions in graphene, $b(\pi) = 0$.

In the long-wavelength regime, $kR \ll 1$, Eq. (38) reduces to

$$\tilde{V}(\mathbf{q}) \simeq -2\pi i \sigma' P \sin\left(\frac{\theta + \phi_{\mathbf{k}}}{2}\right). \quad (42)$$

Assuming also $|E_{\mathbf{k},\sigma}| \gg \Delta$, which effectively corresponds to the gapless case, $\Delta = 0$, the Born approximation yields

$$|f(\theta, \phi_{\mathbf{k}})|^2 = \frac{2\pi k P^2}{v_F^2} \cos^2\left(\frac{\theta - \phi_{\mathbf{k}}}{2}\right) \sin^2\left(\frac{\theta + \phi_{\mathbf{k}}}{2}\right). \quad (43)$$

In this expression, the $\cos^2(\dots)$ factor comes from the ‘‘Dirac factor’’ b in Eq. (41), while the $\sin^2(\dots)$ factor reflects the angular dependence due to the anisotropic electric dipole potential. The transport cross-section, Λ_{tr} , and the total cross-section, Λ , for the massless case then follow from standard definitions,

$$\begin{aligned} \Lambda_{\text{tr}} &= \int_0^{2\pi} d\theta [1 - \cos(\theta - \phi_{\mathbf{k}})] |f(\theta, \phi_{\mathbf{k}})|^2 \\ &= \frac{\pi^2 k P^2}{2v_F^2}, \\ \Lambda &= \int d\theta |f(\theta, \phi_{\mathbf{k}})|^2 = (1 + 2 \sin^2 \phi_{\mathbf{k}}) \Lambda_{\text{tr}}. \end{aligned} \quad (44)$$

Remarkably, the transport cross-section is independent of the incidence angle $\phi_{\mathbf{k}}$. This implies that the dipole-induced angular dependence is precisely compensated by

the ‘‘Dirac factor’’ in Eq. (43), which is responsible for the absence of backscattering. The angle-independent result for Λ_{tr} implies that, as long as the Born approximation is justified, the electrical conductivity remains isotropic even in the presence of arbitrarily oriented static electric dipoles.

4.4 Nonperturbative analysis

We next study the scattering problem for energies approaching the band edges. This requires a nonperturbative analysis, cf. Ref. [42], which we carry out in this subsection by adopting the point-like dipole formulation in Eq. (2). For clarity, we choose $\sigma = -1$, i.e., we write

$$E_{\mathbf{k}} = -\Delta + \epsilon, \quad \epsilon < 0, \quad |\epsilon| \ll \Delta, \quad (45)$$

in what follows. The behavior near the other band edge, $\sigma = +1$, then follows by particle-hole symmetry. Far away from the nuclei, $r \gg R$, the two-center potential is well approximated by the point-like dipole, $V_d = -P \cos(\theta)/r^2$, and the Dirac equation reads

$$\begin{pmatrix} V_d + 2\Delta - \epsilon & e^{-i\theta}(-i\partial_r - \frac{1}{r}\partial_\theta) \\ e^{i\theta}(-i\partial_r + \frac{1}{r}\partial_\theta) & V_d - \epsilon \end{pmatrix} \begin{pmatrix} \eta \\ \chi \end{pmatrix} = 0. \quad (46)$$

To regularize the fall-to-the-center singularity for the $1/r^2$ potential, we impose a boundary condition that forbids particle flow into a disk of radius r_0 around the origin, with a short-distance scale $r_0 \approx R$. In fact, by comparing to the solution of the full two-center problem [28], one finds that the universal bound-state spectrum in Sec. 4.1 is fully recovered from the point-like dipole form with the choice $r_0 = R/4$.

Importantly, the radial and the angular parts can now be separated by mapping the Dirac equation to an equivalent 2D Schrödinger equation. This is a controlled approximation for $P \ll \Delta r_0^2$ and energies near the band edge, $|\epsilon| \ll \Delta$, where the upper spinor component is always small compared to the lower one,

$$\eta(r, \theta) \simeq \frac{e^{-i\theta}}{2\Delta} \left(i\partial_r + \frac{1}{r}\partial_\theta \right) \chi(r, \theta). \quad (47)$$

Under these conditions, Eq. (46) reduces to an effective 2D Schrödinger equation for the lower spinor component only,

$$\left[-\frac{1}{2\Delta} \left(\partial_r^2 + \frac{1}{r}\partial_r + \frac{1}{r^2}\partial_\theta^2 \right) + \frac{P \cos \theta}{r^2} + \epsilon \right] \chi(r, \theta) = 0. \quad (48)$$

The above-mentioned boundary condition at $r = r_0$ then implies a Dirichlet condition for the Schrödinger wavefunction, i.e., $\chi = 0$ for $r < r_0$.

Fortunately, Eq. (48) can now be separated by the Ansatz $\chi(r, \theta) = R(r)Y(\theta)$. With the separation constant γ , the angular function obeys a Mathieu equation,

$$\left(\frac{d^2}{d\theta^2} + \gamma - 2P\Delta \cos \theta \right) Y(\theta) = 0, \quad (49)$$

where 2π -periodic solutions exist only when γ matches one of the characteristic values [23] of the Mathieu equation, $\gamma = \gamma_{j,\kappa}(P\Delta)$. Here, $\kappa = \pm$ is the parity of the solution, $Y_{j,\kappa}(-\theta) = \kappa Y_{j,\kappa}(\theta)$, and $j = 0, 1, 2, \dots$ effectively replaces the conventional angular momentum, with $j + \kappa \geq 0$. The quantum numbers (j, κ) have already appeared in Sec. 4.1, where we discussed the bound-state spectrum, with $\epsilon > 0$ in Eq. (45). Indeed, the angular equation (49) is independent of the particle energy. Following standard notation [23,24], with the Mathieu functions ce_{2j} and se_{2j} , and their respective eigenvalues a_{2j} and b_{2j} , the solutions to Eq. (49) are

$$\begin{aligned} Y_{j,+}(\theta) &= \text{ce}_{2j} \left(\frac{\theta}{2}, 4P\Delta \right), & \gamma_{j,+} &= \frac{1}{4} a_{2j}(4P\Delta), \\ Y_{j,-}(\theta) &= \text{se}_{2j} \left(\frac{\theta}{2}, 4P\Delta \right), & \gamma_{j,-} &= \frac{1}{4} b_{2j}(4P\Delta). \end{aligned} \quad (50)$$

For given dipole moment P , the characteristic values are ordered as $\gamma_{0,+} < \gamma_{1,-} < \gamma_{1,+} < \gamma_{2,-} < \dots$, where $\gamma_{j,\kappa} = -s_{j,\kappa}^2 < 0$ for $P > P_{j,\kappa}$, with $P_{j,\kappa}$ in Eq. (30) [note that $P_{0,+} = 0$] and s_{jk} in Eq. (32). For $P < P_{j,\kappa}$, on the other hand, the respective Mathieu eigenvalue is positive, $\gamma_{j,\kappa} > 0$. With the solution of the angular equation at hand, the radial equation resulting from Eq. (48) becomes a Bessel equation,

$$\left(\frac{d^2}{dr^2} + \frac{1}{r} \frac{d}{dr} - \frac{\gamma_{j,\kappa}}{r^2} + k^2 \right) R_{\mathbf{k},j,\kappa}(r) = 0, \quad (51)$$

where \mathbf{k} , with absolute value $k = \sqrt{-2\Delta\epsilon}$, denotes the incoming momentum of the scattering state. Note that up to this point, the above equations also allow one to study bound-state solutions, see Sec. 4.1 and Ref. [28]. The radial equation now contains a dependence on the dipole moment only through the characteristic values of the Mathieu equation.

The general solution of Eq. (51) can be written in terms of Hankel functions. With complex coefficients $\beta_{\mathbf{k},j,\kappa}$, we obtain

$$R_{\mathbf{k},j,\kappa}(r) \sim \beta_{\mathbf{k},j,\kappa} H_{\sqrt{\gamma_{j,\kappa}}}^{(1)}(kr) + H_{\sqrt{\gamma_{j,\kappa}}}^{(2)}(kr), \quad (52)$$

where $\sqrt{\gamma_{j,\kappa}} \rightarrow is_{j,\kappa}$ for $P > P_{j,\kappa}$, see Eq. (32). For given quantum numbers (\mathbf{k}, j, κ) characterizing the state, the Dirichlet condition at $r = r_0$ now fixes the β coefficients. From now on, we shall focus on the long wavelength regime, $kr_0 \ll 1$, where the short-distance form of the Hankel functions yields

$$\beta_{\mathbf{k},j,\kappa} \simeq \begin{cases} 1, & P < P_{j,\kappa} \\ e^{-\pi s_{j,\kappa}} \frac{\sin[s_{j,\kappa} \ln(ikr_0/2) - \varphi(s_{j,\kappa})]}{\sin[s_{j,\kappa} \ln(-ikr_0/2) - \varphi(s_{j,\kappa})]}, & P > P_{j,\kappa}, \end{cases} \quad (53)$$

with $\varphi(s) = \arg \Gamma(1+is)$. We have thereby constructed the nonperturbative scattering solution of the Dirac equation for $V = V_d$, which holds for energies near the (lower) band edge. For the lower spinor component, we find

$$\chi(r, \theta) = \sum_{j,\kappa} c_{j,\kappa} \left[\beta_{\mathbf{k},j,\kappa} H_{\sqrt{\gamma_{j,\kappa}}}^{(1)}(kr) + H_{\sqrt{\gamma_{j,\kappa}}}^{(2)}(kr) \right] Y_{j,\kappa}(\theta), \quad (54)$$

with complex coefficients $c_{j,\kappa}$. The upper spinor component, $\eta(r, \theta)$, follows by virtue of Eq. (47). The next step is to choose the $c_{j,\kappa}$ to match the asymptotic behavior of Eq. (54) to the general scattering state (34), which then determines the nonperturbative scattering amplitude $f(\theta, \phi_{\mathbf{k}})$.

To that end, we first expand the incoming plane wave in terms of Mathieu functions. Employing the asymptotic form of the radial solution, some algebra yields

$$e^{ikr \cos(\theta - \phi_{\mathbf{k}})} \simeq \sqrt{\frac{2}{\pi i k r}} \sum_{j,\kappa} Y_{j,\kappa}(\theta) \quad (55)$$

$$\times [Y_{j,\kappa}(\phi_{\mathbf{k}}) e^{i k r} + i Y_{j,\kappa}(\phi_{\mathbf{k}} + \pi) e^{-i k r}].$$

This implies that the coefficients $c_{j,\kappa}$ in the scattering state (54) have to be chosen as

$$c_{j,\kappa} = e^{-i(\pi/2)\sqrt{\gamma_{j,\kappa}}} Y_{j,\kappa}(\phi_{\mathbf{k}} + \pi). \quad (56)$$

The scattering amplitude in Eq. (34) is therefore given by

$$f(\theta, \phi_{\mathbf{k}}) = -i \sqrt{\frac{2}{\pi k}} \sum_{j,\kappa} Y_{j,\kappa}(\theta) \quad (57)$$

$$\times [\beta_{\mathbf{k},j,\kappa} e^{-i\pi\sqrt{\gamma_{j,\kappa}}} Y_{j,\kappa}(\phi_{\mathbf{k}} + \pi) - Y_{j,\kappa}(\phi_{\mathbf{k}})].$$

For $P\Delta \rightarrow 0$, this result for the scattering amplitude does not vanish, as may have been expected since the dipole potential is then absent. However, our Dirichlet condition implies the (artificial) presence of an infinitely repulsive hard-wall potential at $r = r_0$, which produces a finite (but spurious) contribution to the scattering amplitude. We have checked that for $P\Delta \rightarrow 0$, Eq. (57) recovers the corresponding isotropic result for the impenetrable radial wall potential, where the scattering amplitude depends only on $\theta - \phi_{\mathbf{k}}$. We stress that there is a separate dependence on θ and $\phi_{\mathbf{k}}$ in the presence of the dipole. However, for all scattering channels (j, κ) not hosting bound states, i.e., as long as $P < P_{j,\kappa}$ and therefore $\gamma_{j,\kappa} > 0$, the choice of the boundary condition is immaterial and one can send $r_0 \rightarrow 0$.

The nonperturbative phenomena of main interest in this subsection involve scattering channels with dipole-induced bound states, i.e., $P > P_{j,\kappa}$. The scattering amplitude (57) then determines the transport cross-section, $A_{\text{tr}}(\phi_{\mathbf{k}})$, and the total cross-section, $\Lambda(\phi_{\mathbf{k}})$, according to the integrals in Eq. (44). Evaluating these integrals numerically, we show typical results in Fig. 3, where the lowest five scattering channels are included. For the shown results, the hard-core contribution due to the Dirichlet boundary condition is negligible against the dipole-induced scattering. The total cross-section in the inset of Fig. 3 exhibits a very similar, π -periodic, angular dependence as the Born approximation result in Eq. (44). However, in marked contrast to the prediction of the Born approximation, the nonperturbative result for the transport cross-section clearly depends on the incidence angle $\phi_{\mathbf{k}}$. This effect can be traced back to the presence of dipole-induced bound states, and directly implies that charge transport

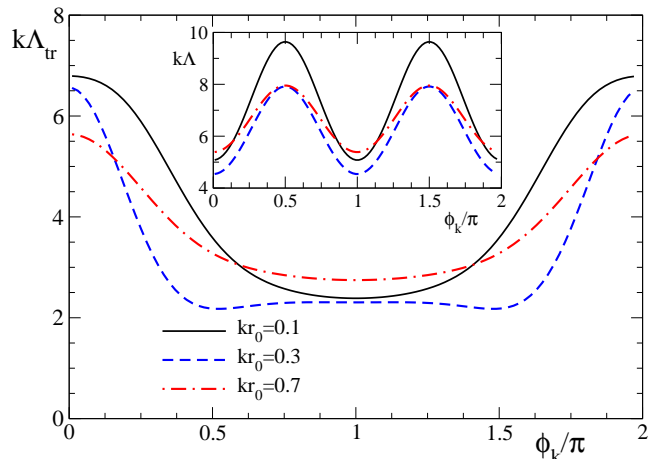


Fig. 3. Main panel: Angular dependence of the transport cross-section A_{tr} vs incidence angle $\phi_{\mathbf{k}}$. The shown results are for dipole moment $P\Delta = 1.05$ and various values of kr_0 . They follow by numerical integration, see Eq. (44), using the non-perturbative scattering amplitude (57). The lowest five (j, κ) scattering channels have been included, and r_0 can be identified with $R/4$, where R is the distance between the Coulomb centers. Inset: Same but for the total cross-section Λ .

properties will be angle-dependent at energies approaching the edge, $|E_{\mathbf{k},\sigma}| \rightarrow \Delta$, where the Born approximation breaks down.

5 Conclusions

In this paper, we have discussed several noteworthy features of Dirac fermions in graphene in the presence of a two-center potential. For equal nuclear charges of slightly subcritical value, one can induce a transition to the supercritical regime by lowering the distance R between the Coulomb centers below a critical value R_{cr} . Our LCAO predictions for the ground-state energy are qualitatively similar to previous results obtained by an asymptotic matching approach [19].

For opposite charges, the potential at large distances is equivalent to a static electric dipole potential. In graphene, even a very weak dipole can capture infinitely many bound states, and we have addressed the corresponding scattering problem in some detail. For energies not too close to the band edge, the Born approximation is valid and predicts that the transport cross-section is isotropic. This conclusion can be rationalized by noting that the dipolar angular dependence is precisely compensated by the one due to the Dirac nature of the quasi-particles in graphene. Important deviations from the Born approximation originate from scattering channels that are linked to bound states. Note that there is at least one infinite tower of bound states for arbitrary dipole strength. We have determined a nonperturbative solution for the scattering amplitude within a point-like dipole model, which indicates that

a nontrivial angular dependence of the transport cross-section will be present as a consequence of such effects.

To conclude, we hope that our predictions can soon be probed experimentally by scanning tunneling spectroscopy on graphene monolayers along the lines of Refs. [13, 16, 17].

We thank A. Altland, E. Andrei, J.-C. Cuenin, H. Siedentop, and A. Zazunov for valuable discussions. Financial support by the DFG (SFB TR12 and SPP 1459) and by the Volkswagen-Stiftung is gratefully acknowledged.

References

1. A.H. Castro Neto, F. Guinea, N.M.R. Peres, K.S. Novoselov, A. Geim, *Rev. Mod. Phys.* **81**, 109 (2009).
2. M.A.H. Vozmediano, M.I. Katsnelson, F. Guinea, *Phys. Rep.* **496**, 109 (2010).
3. D. Huertas-Hernando, F. Guinea, A. Brataas, *Phys. Rev. B* **74**, 155426 (2006).
4. V.N. Kotov, B. Uchoa, V.M. Pereira, A.H. Castro Neto, F. Guinea, *Rev. Mod. Phys.* **84**, 1067 (2012).
5. L.A. Ponomarenko, R.V. Gorbachev, G.L. Yu, D.C. Elias, R. Jalil, A.A. Patel, A. Mishchenko, A.S. Mayorov, C.R. Woods, J.R. Wallbank, M. Mucha-Kruczynski, B.A. Piot, M. Potemski, I.V. Grigorieva, K.S. Novoselov, F. Guinea, V.I. Fal'ko, A.K. Geim, *Nature* **497**, 594 (2013).
6. J.C.W. Song, A.V. Shytov, L.S. Levitov, *Phys. Rev. Lett.* **111**, 266801 (2013).
7. V. Khalilov, H. Choon-Lin, *Mod. Phys. Lett. A* **13**, 615 (1998).
8. D.S. Novikov, *Phys. Rev. B* **76**, 245435 (2007).
9. V.M. Pereira, J. Nilsson, A.H. Castro Neto, *Phys. Rev. Lett.* **99**, 166802 (2007).
10. A.V. Shytov, M.I. Katsnelson, L.S. Levitov, *Phys. Rev. Lett.* **99**, 246802 (2007).
11. O.V. Gamayun, E.V. Gorbar, V.P. Gusynin, *Phys. Rev. B* **80**, 165429 (2009).
12. D. Klöpfer, A. De Martino, R. Egger, *Crystals* **3**, 14 (2013).
13. Y. Wang, V.W. Brar, A.V. Shytov, Q. Wu, W. Regan, H.-Z. Tsai, A. Zettl, L.S. Levitov, M.F. Crommie, *Nature Physics* **8**, 653 (2012).
14. W. Greiner, B. Müller, J. Rafelski, *Quantum electrodynamics of Strong Fields* (Springer, Berlin, 1985).
15. V.S. Popov, *Phys. At. Nucl.* **64**, 367 (2001).
16. A. Luican-Mayer, M. Kharitonov, G. Li, C.P. Lu, I. Skachko, A.M.B. Goncalves, K. Watanabe, T. Taniguchi, E.Y. Andrei, *Phys. Rev. Lett.* **112**, 036804 (2014).
17. Y. Wang, D. Wong, A.V. Shytov, V.W. Brar, S. Choi, Q. Wu, H.-Z. Tsai, W. Regan, A. Zettl, R.K. Kawakami, S.G. Louie, L.S. Levitov, M.F. Crommie, *Science* **340**, 734 (2013).
18. C. Cohen-Tannoudji, B. Diu, and F. Laloë, *Quantum Mechanics*, Vol. 2 (Hermann, Paris, France, 1977).
19. O.O. Sobol, E.V. Gorbar, V.P. Gusynin, *Phys. Rev. B* **88**, 205116 (2013).
20. S.S. Gerstein and Ya.B. Zeldovich, *Sov. Phys. JETP* **30**, 358 (1970).
21. J. Rafelski, L.P. Fulcher, and W. Greiner, *Phys. Rev. Lett.* **27**, 958 (1971).
22. Ya.B. Zeldovich and V.N. Popov, *Sov. Phys. Usp.* **14**, 673 (1972).
23. I.S. Gradshteyn, I.M. Ryzhik, *Table of Integrals, Series, and Products* (Academic Press, Elsevier, 2007).
24. M. Abramowitz, I.A. Stegun (eds.), *Handbook of Mathematical Functions* (Dover, New York, 1965).
25. V. Matveev, D. Matrasulov, H. Rakhimov, *Phys. At. Nucl.* **63**, 318 (2000).
26. V.V. Bondarchuk, I.M. Shvab, D.I. Bondar, A.V. Kater-noga, *Phys. Rev. A* **76**, 062507 (2007).
27. V.M. Pereira, A.H. Castro Neto, H.Y. Liang, L. Mahadevan, *Phys. Rev. Lett.* **105**, 156603 (2010).
28. A. De Martino, D. Klöpfer, D. Matrasulov, R. Egger, *Phys. Rev. Lett.* **112**, 186603 (2014).
29. D.I. Abramov, I.V. Komarov, *Theor. Math. Phys.* **13**, 209 (1972).
30. D.U. Matrasulov, V.I. Matveev, M.M. Musakhanov, *Phys. Rev. A* **60**, 4140 (1999).
31. H.E. Camblong, L.N. Epele, H. Fanchiotti, C.A.G. Canal, *Phys. Rev. Lett.* **87**, 220402 (2001).
32. K. Connolly, D.J. Griffiths, *Am. J. Phys.* **75**, 527 (2007).
33. D. Schumayer, B.P. Zyl, R.K. Bhadure, D.A.W. Hutchinson, *EPL* **89**, 13001 (2010).
34. K.K. Gomes, W. Mar, W. Ko, F. Guinea, H.C. Manoharan, *Nature* **483**, 306 (2012).
35. M.Z. Hasan, C.L. Kane, *Rev. Mod. Phys.* **82**, 3045 (2010).
36. J.-C. Cuenin, H. Siedentop, preprint arXiv:1403.7160.
37. V. Efimov, *Phys. Lett. B* **33**, 563 (1970).
38. E. Braaten and H.W. Hammer, *Phys. Rep.* **428**, 259 (2007).
39. A.O. Gogolin, C. Mora, and R. Egger, *Phys. Rev. Lett.* **100**, 140404 (2008).
40. A.A. Perelomov, V.S. Popov, *Theor. Math. Phys.* **4**, 664 (1970).
41. A. Zazunov, A. Kundu, A. Hütten, R. Egger, *Phys. Rev. B* **82**, 155431 (2010).
42. W.R. Garrett, *Phys. Rev. A* **4**, 2229 (1971).